Control and synchronization of spatiotemporal chaos

Alexander Ahlborn and Ulrich Parlitz
Drittes Physikalisches Institut, Universität Göttingen, Friedrich-Hund-Platz 1, 37077 Göttingen, Germany
(Received 19 September 2007; published 7 January 2008)

Chaos control methods for the Ginzburg-Landau equation are presented using homogeneously, inhomogeneously, and locally applied multiple delayed feedback signals. In particular, it is shown that a small number of control cells is sufficient for stabilizing plane waves or for trapping spiral waves, and that successful control is closely connected to synchronization of the dynamics in regions close to the control cells.

DOI: 10.1103/PhysRevE.77.016201 PACS number(s): 05.45.Gg

I. INTRODUCTION

Turbulent motion like irregular wave fronts or chaotic spiral waves are a widespread phenomenon in spatiotemporal systems [1–8]. From the physicist's point of view such dynamics is interesting to analyze but for technological processes like electrocatalysis in fuel cells, corrosion, electrochemical machining of metals, etc. spatiotemporal chaos is often unwanted or even harmful. Another example where chaos may occur in an undesired way is the human heart. As a result of irregularities or desease the (almost) plane waves normally traveling around the heart muscle may split up into several coexisting (chaotic) spiral waves leading to arrythmias like irregular oscillations or fibrillation [6].

Thus for all these examples strategies are required to manipulate and control the system of interest. The different approaches [9] to tame spatiotemporal chaos suggested during the past decade can be classified as static and dynamic methods. Static methods take advantage of the influence of boundary conditions or additionally inserted small inhomogeneities [10,11]. Dynamic control techniques, on the other hand, may be subdivided into open and closed loop methods. Open loop control may be implemented, for example, as external periodic forcing [12–14] or in terms of short pulses used to eliminate spiral waves in cardiac tissue and to reset human heart muscle contractions [15]. More efficient (but also more difficult to realize) are closed loop control schemes where in general a system of the type

$$\dot{\mathbf{x}} = \mathbf{f}(\mathbf{x},\mathbf{u}) \tag{1}$$

is controlled by a signal $\mathbf{u}$ that depends on the state $\mathbf{x}$ and the goal dynamics. This class of feedback control methods includes proportional control using one or more suitably chosen observables of the considered system [16] or delayed feedback control (DFC) like Pyragas' *time delay auto synchronization* (TDAS),

$$\mathbf{u} = k[\mathbf{g}(\mathbf{x}(t-\tau)) - \mathbf{g}(\mathbf{x}(t))], \tag{2}$$

based on the difference of some observable $\mathbf{g}(\mathbf{x}(t))$ and its delayed value $\mathbf{g}(\mathbf{x}(t-\tau))$ amplified by a common (symmetric) gain factor k [17]. The efficiency for stabilizing unstable periodic orbits (UPOs) can be further improved by also including integer multiples of the fundamental delay time τ in the feedback signal [18]. This *extended TDAS* (ETDAS) as well as TDAS has been used to control various dynamical systems including spatially extended ones [19–23], where additional spatial filtering of the control signal may be used to further improve the performance [24]. For spatiotemporal systems the application of the resulting feedback can be either local or global using, e.g., a mean field signal.

In contrast to (E)TDAS based on a single delay time only and symmetric gain factors, it has been shown recently that stabilization of steady states (fixed points) can significantly be improved by multiple delay feedback control (MDFC) based on control signals with two or more independent delay times where the corresponding terms are weighted by asymmetric gains [25]. Successful applications of MDFC comprise several theoretical [26,27] and experimental systems like the suppression of irregular intensity fluctuations of intracavity frequency doubled solid state lasers [25,28] where chaos limits technical applications (e.g., holographic displays) requiring constant light output. Furthermore, it has been shown for the two-dimensional Ginzburg-Landau equation that (homogenous) MDFC with asymmetric gains can bypass some severe limitations valid for (E)TDAS in connection with the stabilization of the so-called saddle points [29].

In the following, we shall discuss different cases of spatially extended control schemes starting in Sec. II A with homogeneous control where the control signal is applied everywhere in space in the same way. This case can be treated analytically (to some extent) and we shall demonstrate that MDFC with asymmetric gains provides extended stability regions of (unstable) plane wave solutions. Then in Sec. II B the case of inhomogeneous control is investigated with control gain factors varying periodically in space. In this way some perturbed plane waves can be stabilized as will be shown by a semianalytic study. These investigations pave the way to local control (Sec. II C) where the control signal is applied at some control cells, only. This case is relevant for most experimental implementations and will be investigated by numerical simulations. Examples of stabilized plane waves and trapped spirals will be given, illustrating possible applications of local MDFC to spatiotemporal chaos. Successful control is accompagnied by synchronization phenomena between the coupled control cells. This aspect will be investigated in Sec. III.

II. FEEDBACK CONTROL

As a prototypical example of a spatiotemporal system we consider the two-dimensional complex Ginzburg-Landau equation (GLE)

 ©2008 The American Physical Society

$$\partial_t f = (1+ia)\nabla^2 f + f - (1+ib)f|f|^2 + g(\mathbf{x})u \tag{3}$$

with an external control signal $u(\mathbf{x},t)$ that is applied with a spatially varying gain function $g(\mathbf{x})$. ∂_t and ∇ denote the temporal and the spatial derivative, respectively. The free running system ($u=0$) possesses an unstable steady state $[f(\mathbf{x},t)=0]$ that can be stabilized by means of a proportional controller or MDFC. Furthermore, harmonic waves

$$f(\mathbf{x},t) = f_0 e^{i(\mathbf{k_0}\cdot\mathbf{x}-\omega_0 t)} \tag{4}$$

with wave vector $\mathbf{k_0}$, frequency ω_0, and amplitude f_0 comprise unstable solutions of the free running GLE (3) [30]. Substituting the harmonic waves [Eq. (4)] into the GLE (3) yields relations $\omega_0 = k_0^2(a-b)+b$ and $f_0 = \sqrt{1-k_0^2}$ with $k_0^2 = \|\mathbf{k_0}\|^2 \leqslant 1$. These unstable waves are unstable periodic orbits (UPOs) that we want to stabilize by suitable feedback control.

A. Homogeneous feedback

First, for completeness we revisit the case of *homogeneous feedback* where $g(\mathbf{x})=1$ [29]. To stabilize plane waves [Eq. (4)] we use the MDFC signal

$$u(\mathbf{x},t) = \sum_{m=1}^{M} k_{ma} f(\mathbf{x}, t-\tau_m) - k_{mb} f(\mathbf{x},t) \tag{5}$$

with gains k_{ma}, k_{mb} and delay times τ_m. Here, we assume that the controlled plane wave is given as $f(\mathbf{x},t)=f_c e^{i(\mathbf{k_c}\cdot\mathbf{x}-\omega_0 t)}$, i.e., it possesses the same frequency ω_0 as the free running wave but different wave number k_c and amplitude f_c. If this plane wave is substituted into Eq. (5) one obtains $u(\mathbf{x},t)=T(\omega_0)f(\mathbf{x},t)$ with transfer function $T(\omega_0) = \sum_{m=1}^{M} k_{ma} e^{-i\omega_0\tau_m} - k_{mb}$. Inserting the plane wave solution and the corresponding control term into the GLE (3) results in

$$\begin{aligned} 1 - k_c^2 - f_c^2 + \mathrm{Re}[T(\omega_0)] &= 0, \\ \omega_0 - a k_c^2 - b f_c^2 + \mathrm{Im}[T(\omega_0)] &= 0, \end{aligned} \tag{6}$$

where $k_c^2 = \|\mathbf{k_c}\|^2$. Combining both constraints of Eq. (6) we obtain the dispersion relation

$$k_c^2 = k_0^2 + \Delta k^2 \tag{7}$$

where

$$\Delta k^2 = \frac{b\,\mathrm{Re}[T(\omega_0)] - \mathrm{Im}[T(\omega_0)]}{b-a} \tag{8}$$

describes the *wave number shift* due to the feedback control. Since $k_0^2 \leqslant 1$ the relation $k_c^2 \geqslant 0$ is fulfilled if $\Delta k^2 \geqslant -1$. The wave number shift Δk^2 vanishes if the condition $b\,\mathrm{Re}[T(\omega_0)] = \mathrm{Im}[T(\omega_0)]$ holds and in this case control results in a plane wave with the same wave number $k_c = k_0$ as for the free running system but different amplitude $f_c = \sqrt{f_0^2 + \mathrm{Re}[T(\omega_0)]}$.

The magnitude of the wave number shift depends on the transfer function $T(\omega_0)$ that can be adjusted with the parameters k_{ma} and k_{mb} of the control signal. To illustrate this dependence we show in Figs. 1(a) and 1(b) the value of Δk^2 (grayscaled) in the control parameter plane $\tau_1 - k_{1b}$ for MDFC with one and two delay times, respectively. Below some critical values of the gain k_{1b} control fails and the plane wave remains unstable (light gray shading in Fig. 1). Since the parameter values of the GLE are in this case $a=1.1$ and $b=-1$ the TDAS controllability criterion $ab > -1$ derived in Ref. [30] is *not* fulfilled. Therefore symmetric delayed feedback control with $k_{1a}=k_{1b}$ fails as can also be seen in Fig. 1(a) where the dashed line at $k_{1b}=0.4=k_{1a}$ lies in the unstable region. In contrast, asymmetric delayed feedback enables stabilization if the gain k_{1b} is sufficiently high, including parameter combinations (τ_1, k_{1b}) where Δk^2 vanishes.

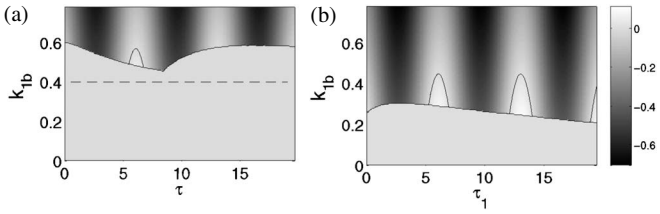

FIG. 1. Stabilization of plane wave solutions of the GLE (3) with $a=1.1$ and $b=-1$ using the delayed feedback signal (5). In the grayshaded regions of the control parameter space $\tau_1 - k_{1b}$ stabilization is successful and results in the grayscaled wave number shift Δk^2 [Eq. (8)] vanishing for parameter combinations indicated by the $\cap$-shaped curves. (a) Single delay feedback with $k_{1a}=0.4$. The dashed line denotes the case of symmetric feedback ($k_{1a}=k_{1b}$) that fails to stabilize plane waves. (b) MDFC with two delay times and fixed control parameters $k_{1a}=0.4$, $k_{2a}=0.2$, $k_{2b}=0.4$, and $\tau_2=6.2$.

Similar to the results obtained with several other dynamical systems [25,27] application of an additional feedback loop with a different delay time $\tau_2=6.2$ results in increasing stability, here visible as a reduced size of the unstable region shown in Fig. 1(b).

B. Inhomogeneous feedback

We shall now consider the case where the strength of the control signal depends on the spatial location. This kind of *inhomogeneous feedback* can be modeled by means of a gain function $g(\mathbf{x})$ varying in space. The controlled plane waves

$$f(\mathbf{x},t) = f_c e^{i[\mathbf{k_c}\cdot\mathbf{x}+h(\mathbf{x})-\omega_0 t]} \tag{9}$$

are now not purely harmonic anymore but contain some *phase function* $h(\mathbf{x})$. Inserting Eq. (9) into the GLE (3) leads to

$$\begin{aligned} 1 - (k_c + h')^2 - f_c^2 - a h'' + g(\mathbf{x})\mathrm{Re}[T(\omega_0)] &= 0, \\ \omega_0 - a(k_c + h')^2 - b f_c^2 + h'' + g(\mathbf{x})\mathrm{Im}[T(\omega_0)] &= 0. \end{aligned} \tag{10}$$

Here again we may eliminate f_c^2 and obtain with the abbreviation $c=(a-b)/(1+ab)$ an ordinary differential equation

$$\frac{1}{c} h''(\mathbf{x}) = [k_c + h'(\mathbf{x})]^2 - [k_0^2 + g(\mathbf{x})\Delta k^2] \tag{11}$$

for the phase function $h(\mathbf{x})$ where Δk^2 is the wave number shift as defined in Eq. (8). Equation (11) can be transformed

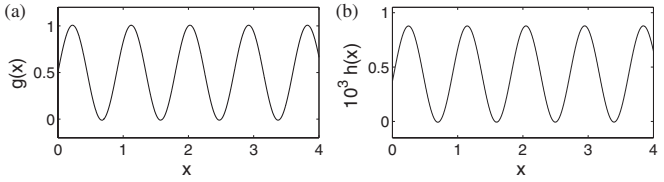

FIG. 2. (a) Sinusoidally modulated gain function $g(x)=0.5+0.5\sin(0.9x)$. (b) Resulting phase function $h(x)$ obtained by numerical integration of the ODE (11) with $k_c=1$, $k_0=0.9$, and $\Delta k^2=-0.32$.

with $H(\mathbf{x})=k_c+h'(\mathbf{x})$ into the *Riccati differential equation*

$$H'(\mathbf{x}) = cH^2(\mathbf{x}) - c[k_0^2 + g(\mathbf{x})\Delta k^2] \tag{12}$$

for which, unfortunately, no general analytical solution exists.

For the special case $b\,\mathrm{Re}[T(\omega_0)]=\mathrm{Im}[T(\omega_0)]$, however, the wave number shift Δk^2 vanishes and Eq. (11) [or equivalently, Eq. (12)] provides steady state solutions $h_1(\mathbf{x})=\varphi_1$ and $h_2(\mathbf{x})=-2k_0\mathbf{x}+\varphi_2$ where φ_1 and φ_2 denote constant phases, respectively. The resulting controlled waves

$$f_1(\mathbf{x},t) = f_c e^{i[\mathbf{k_c}\cdot\mathbf{x}+h_1(\mathbf{x})-\omega_0 t]} = f_c e^{i(\mathbf{k_0}\cdot\mathbf{x}+\varphi_1-\omega_0 t)}$$

and

$$f_2(\mathbf{x},t) = f_c e^{i[\mathbf{k_c}\cdot\mathbf{x}+h_2(\mathbf{x})-\omega_0 t]} = f_c e^{i(-\mathbf{k_0}\cdot\mathbf{x}+\varphi_2-\omega_0 t)}$$

represent harmonic waves running in opposite directions. Similar to the case of homogeneous feedback, here control succeeds to stabilize a plane wave with the same frequency ω_0 and the same wave number $k_c=k_0$ as for the free running system. The amplitude, however, $f_c(\mathbf{x})=\sqrt{f_0^2+g(\mathbf{x})\mathrm{Re}[T(\omega_0)]}$ is now not only different from the amplitude f_0 of the free running system but also varies in space [by an amount that can be minimized by choosing suitable parameters k_{ma}, k_{mb}, and τ_m of the transfer function $T(\omega_0)$].

To analyze the influence of the gain function $g(\mathbf{x})$ for $\Delta k \neq 0$ we shall now consider the one-dimensional case. Our first example consists of a sinusoidal modulation of the gain $g(x)=0.5+0.5\sin(k_g x)$ with $k_g=0.9$. Numerical solution of the Ricatti ordinary differential equation (ODE) (12) provides an almost harmonic phase function $h(x)$ as shown in Fig. 2. This periodic solution $h(x)$ is a stable limit cycle of ODE (11) attracting solutions from a large basin of initial conditions.

Since it is difficult to find an analytic solution for a given gain function we shall now go in the opposite direction starting from a given phase function $h(x)=\varphi_0+\varepsilon\sin(k_p x+\varphi)$ that is substituted into the ODE (11) to obtain the corresponding gain function

$$g(x) = \gamma + \delta\left[\frac{2\varepsilon}{\alpha}\sin(k_p x+\varphi) + \frac{4\varepsilon k_c}{k_p}\cos(k_p x+\varphi) + \varepsilon^2\cos(2k_p x+2\varphi)\right] \tag{13}$$

with $\gamma=(2k_c^2+\varepsilon k_p^2-k_0^2)/(2\Delta k^2)$ and $\delta=k_p^2/(2\Delta k^2)$. Here, a higher harmonic with doubled wave number $2k_p$ occurs which is, however, dominated by the (fundamental) harmonic components if the modulation amplitude ε of the phase function is small. Thus the numerical as well as the analytical example show that (almost) sinusoidal gain functions are associated to (almost) sinusoidal phase functions.

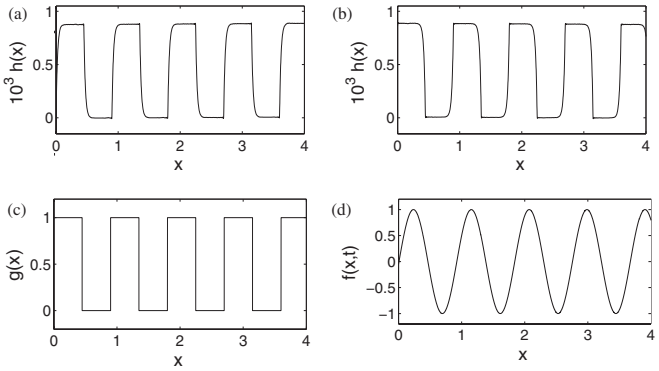

FIG. 3. (a) Periodic rectangular gain function activating and deactivating control in different spatial locations. (b) and (c) Coexsting (stable) solutions of the ODE (12) for different intial conditions providing phase functions $h(x)$ corresponding to waves running in opposite directions. (d) Magnitude of the resulting solution of the one-dimensional GLE (3).

Our third one-dimensional example is again based on a numerical solution of ODE (11), but now for a periodic rectangular gain function shown in Fig. 3(a). This gain function g takes values of one and zero, only, i.e., it switches control on and off depending on the spatial location. Figures 3(a) and 3(b) show numerically computed phase functions $h(x)$ corresponding to waves running to the left or to the right. The magnitude of the solution $f(x,t)$ of the GLE (3) shown in Fig. 3(d) for a fixed time t still is very close to a sinusoidal function.

C. Local feedback

The previous example with a rectangular gain function is motivated by the fact that in experimental systems it is often very difficult (or even impossible) to apply a control signal everywhere in space. Returning to the two-dimensional GLE we shall therefore now consider cases where the control signal is measured and applied in some local *control cells* $\mathcal{C}_j$, only, centered at the points $\mathbf{x_j}$ [29,31]. The measured signal $s_j(t)$ from control cell $\mathcal{C}_j$ is given by

$$s_j(t) = \int_{\mathcal{C}_j} f(\mathbf{z},t)d\mathbf{z}. \tag{14}$$

In general, measured signals are input variables of the feedback loop applied to the same or other control cells. If feedback to the same cell is implemented (simplest case) then the control signal for cell $\mathcal{C}_j$ reads

$$u_j(t) = \sum_{m=1}^{M} k_{ma}s_j(t-\tau_m) - k_{mb}s_j(t) \tag{15}$$

with gains k_{ma}, k_{mb} and delay times τ_m.

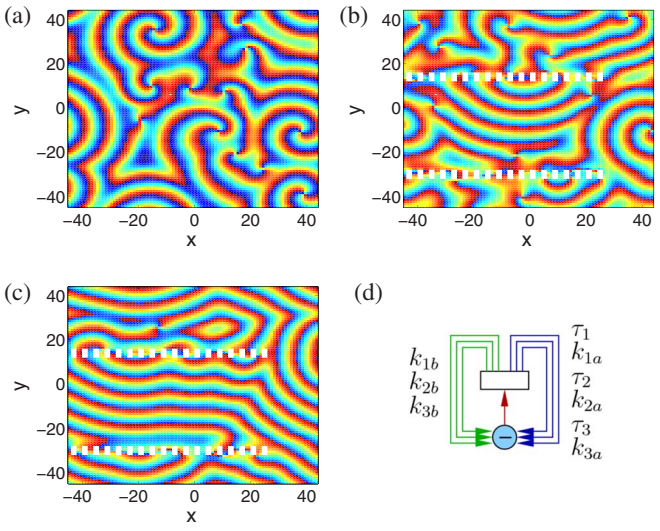

FIG. 4. (Color online) Grayscaled phase dynamics [32] of the complex solution f of the two-dimensional GLE (3). The chaotic spiral wave motion occuring for the system running without control (a) is converted via transients (b) into traveling plane waves (c) (asymptotic dynamics). Here, signals from each control cell (white rectangles) are fed back to the same cell with and without delay using control signal (15) as illustrated in (d).

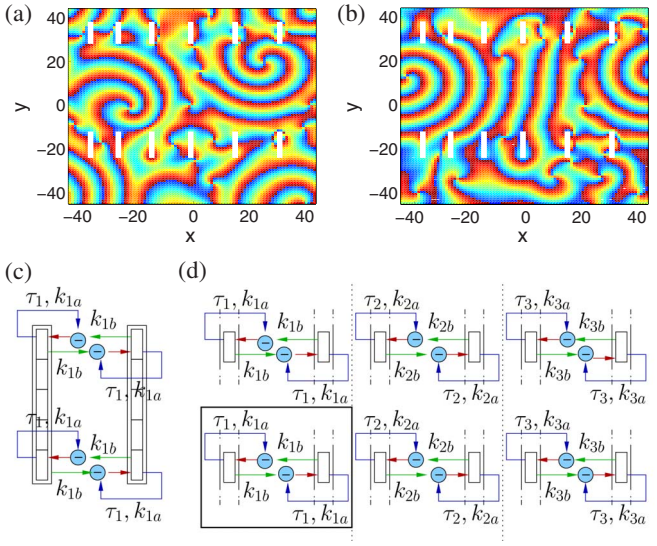

FIG. 5. (Color online) Grayscaled phase dynamics [32] of the controlled GLE (3) governed by the generation and annihilation of plane waves. (a) Transient phase with two counter-rotating spirals. (b) Asymptotic controlled dynamics. (c) Coupling of control cells located in a pair of line segments [marked in white in (a) and (b)]. (d) Pairs of line segments as used in (a) and (b) with control parameter values given in the text.

For controlled plane waves (9) the feedback signal simplifies to

$$u_j(t) = T(\omega_0)s_j(t), \tag{16}$$

where $T(\omega_0)=\Sigma_{m=1}^{M} k_{ma}e^{-i\omega_c\tau_m}-k_{mb}$ denotes the transfer function of the control signal.

For most applications it is preferable to use as few control cells as possible in order to reduce the effort needed to achieve the considered goal dynamics. If, on the other hand, too few, and therefore, widely separated control cells are used, a phenomenon similar to diffraction occurs without any significant influence of the feedback on the chaotic dynamics. The critical distance of control cells is given by the spatial correlation length C_{xy}, which coincides to plane waves with the wavelength $\lambda_c=2\pi/k_c$. A region can be controlled if it is covered with control cells whose mutual distance is less than or equal to C_{xy}.

Figure 4 shows an example of the local multiple delay feedback control approach. Here the GLE (3) is integrated numerically using a fourth order Runge-Kutta solver in time and a spectral method in space which is devided into 90×90 cells with $\Delta x=\Delta y=1$. Figure 4(a) shows the chaotic spiral dynamics generated by the uncontrolled ($u=0$) GLE (3) for $a=-1.45$ and $b=0.34$. After activation of the local control Eq. (15) at the control cells marked in white a transient takes place that is shown in Fig. 4(b) and finally plane waves run between the two rows of control cells as shown in Fig. 4(c). The local coupling is given by Eq. (15) and illustrated in Fig. 4(d). Control parameters are the delay times $\tau_1=21$, $\tau_2=59$, and $\tau_3=94$ and the gains $k_{1a}=0.23$, $k_{2a}=0.4$, $k_{3a}=0.1$, $k_{1b}=0.43$, $k_{2b}=0.48$, and $k_{3b}=0.1$. The size of the control cells is $a_x=C_{xy}/4$, $a_y=C_{xy}/2$, and their horizontal distance equals $d_x=C_{xy}/2$. With these control parameter values plane waves are finally stabilized between the two rows of control cells.

For the previous example we applied individual MDFC at each cell, i.e., signals from a given control cell $\mathcal{C}_j$ were used to control the same cell [Fig. 4(d)]. More sophisticated MDFC couplings combine (delayed) signals from different cells, where, for example, signals are measured at control cell $\mathcal{C}_p$ and applied to cell $\mathcal{C}_q$.

An example for such an interconnected coupling is given in Fig. 5 for chaotic spiral dynamics [similar to Fig. 4(a)] generated by the free running GLE (3) with parameters $a=-1.45$ and $b=0.34$. The control cells (same size as in Fig. 4) are grouped in small vertical line segments as shown in Fig. 5(c). Pairs of cells opposite to each other [Fig. 5(c)] are mutually coupled using the control signal

$$u_{pr}(t) = k_{ma}s_{pr}(t-\tau_m) - k_{mb}s_{pl}(t) \tag{17}$$

for the right control cell and

$$u_{pl}(t) = k_{ma}s_{pl}(t-\tau_m) - k_{mb}s_{pr}(t) \tag{18}$$

for the corresponding left cell. The delay time τ_m and the gains k_{ma} and k_{mb} are the same for all cells in a given pair of line segments [Fig. 5(c)], but differ for the three pairs of segments in both rows as illustrated in Fig. 5(d). With the control parameters $k_{1a}=0.11$, $k_{2a}=0.25$, $k_{3a}=0.32$, $k_{1b}=0.27$, $k_{2b}=0.2$, $k_{3b}=0.39$, $\tau_1=57$, $\tau_2=29$, and $\tau_3=79$ two counter-rotating spirals occur during the transient phase [Fig. 5(a)] but turn out to be unstable and finally, only one spiral survives due to competing dynamics. The asymptotic behavior is some sort of wave baseball where wave fronts emitted by one spiral (pitcher) are straightened under the influence of

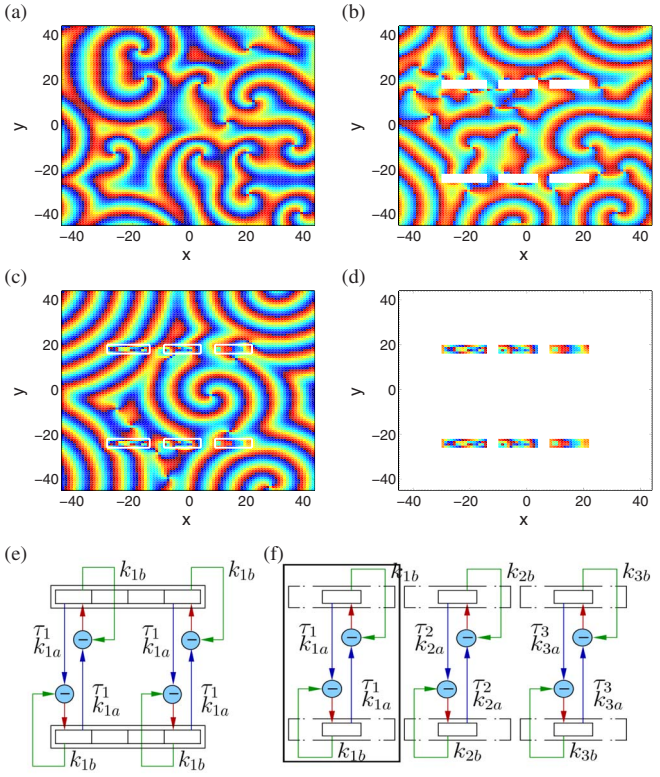

FIG. 6. (Color online) Grayscaled phase dynamics [32] of the GLE (3) for $a=-1.45$ and $b=0.34$. Using the coupling scheme (e) and (f) a rotating spiral wave is trapped. (a) Chaotic spiral waves without control, (b) control transient, and (c) asymptotic controlled dynamics. Marked is the envelope of the line segments each consisting of various control cells of size $a_x=C_{xy}/4$, $a_y=C_{xy}/2$ for the three delay times τ_m. (d) Detailed view of the region of control cells synchronized within the upper and lower line segments. Parameters of the control scheme are given in the text.

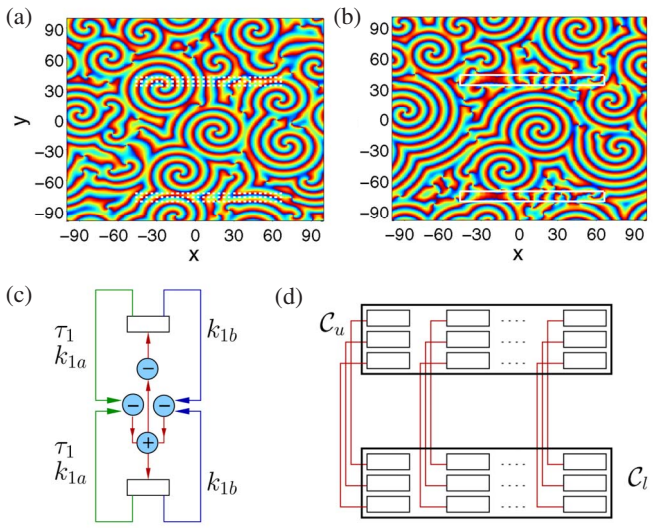

FIG. 7. (Color online) Identical synchronization of the GLE (3) for $a=-1.45$ and $b=0.34$. Groups of control cells bidirectionally coupled by signals (20) and (21) are positioned in two facing line segments. (a) Transient dynamics showing the position of the control cells (marked in white) with size $a_x=a_y=C_{xy}/4$. (b) Synchronized asymptotic dynamics within the region of line segments whose envelope is plotted as a white rectangle. (c) Pairwise coupling scheme of control cells. (d) Locations of coupled pairs of control cells within the line segment shown in (a).

feedback and then caught up by the next spiral (catcher) visible in Fig. 5(b) (actually, due to the periodic boundary condition, the emitting and the receiving spiral are the same).

To stabilize one of the spirals occuring during the transient phase the control setup of Fig. 5(c) has to be modified to the one shown in Fig. 6(e). Now three vertical pairs of line segments with control cells are used and the mutual coupling of opposite cells is shown in Fig. 6(e). Again, each pair of line segments is characterized by its own control parameter set as indicated in Fig. 6(f). For control parameters $k_{1a}=0.22$, $k_{2a}=0.1$, $k_{3a}=0.35$, $k_{1b}=0.3$, $k_{2b}=0.5$, $k_{3b}=0.0$, $\tau_1=41$, $\tau_2=27$, and $\tau_3=19$ a spiral is trapped [Fig. 6(c)] after some transient [Fig. 6(b)]. Here, the control signals for the upper and lower cells are written as

$$u_{pu}(t) = k_{ma}s_{pl}(t-\tau_m) - k_{mb}s_{pu}(t),$$

$$u_{pl}(t) = k_{ma}s_{pu}(t-\tau_m) - k_{mb}s_{pl}(t). \tag{19}$$

The rotation direction of the spiral wave trapped in the control region can be manipulated by changing the feedback parameters. Furthermore, it is important to choose the spatial distance of complementary control cells within a certain range, so that spiral waves have enough space to develop. If the controlled region is chosen too large or too small several spiral waves or other turbulent structures occur. Figure 6(d) shows the dynamics within the control segments [also visible in Fig. 6(c)]. As can be seen, the same pattern occurs in corresponding (i.e., coupled) control cells and the applied control thus results in a *synchronization* of the control cell dynamics. This aspect will be discussed in the next section.

III. SYNCHRONIZATION

To investigate the synchronization of different regions of the controlled GLE (3) we now consider a larger spatial grid of 200×200 cells ($\Delta x=\Delta y=1$). Parameters are $a=-1.45$ and $b=0.34$. Signals needed to achieve control/synchronization are again applied via control cells. To guarantee a large spatial separation, these control cells are aligned in two facing line segments [see Figs. 7(b) and 7(d)] in a vertical distance corresponding to the tenfold of the spatial correlation length C_{xy}. Within these line segments control cells of size $a_x=C_{xy}/4$ and $a_y=C_{xy}/4$ are located in a horizontal and vertical distance of $d_x=C_{xy}/2$ and $d_y=C_{xy}/2$, respectively [see Figs. 7(a) and 7(d)]. Control cells $\mathcal{C}_u$ of the upper segment can interact with corresponding cells $\mathcal{C}_l$ of the lower segment via control signals

$$u_u = k_{1b}[s_l(t) - s_u(t)] + k_{1a}[s_l(t-\tau) - s_u(t-\tau)], \tag{20}$$

$$u_l = k_{1b}[s_u(t) - s_l(t)] + k_{1a}[s_u(t-\tau) - s_l(t-\tau)] \tag{21}$$

that are applied to the correspoding upper and lower cells, respectively. Here, $s_u(t)$ and $s_l(t)$ denote locally averaged sig-

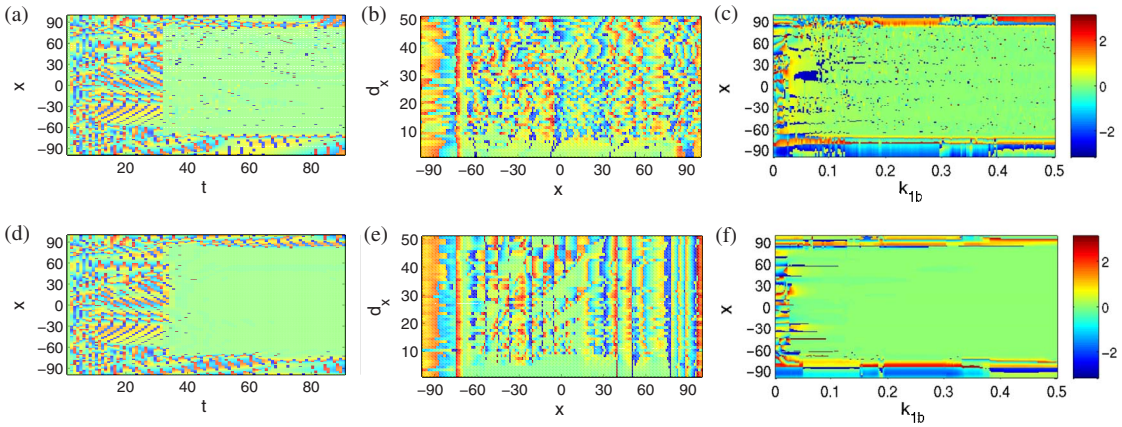

FIG. 8. (Color online) Identical synchronization of the GLE (3) between horizontal sections of the lower and upper line segments of control cells shown in Fig. 7. Control is activated for $t>30$. (a)–(c) Bidirectional coupling using Eqs. (20) and (21) and (d)–(f) unidirectional coupling (20). (a),(d) Temporal evolution of the (grayscaled) synchronization error (22). (b),(e) Dependence of the (asymptotic) synchronization error on the horizontal distance of control cells d_x. (c),(f) Dependence of the (asymptotic) synchronization error on the feedback gain k_{1b} where $k_{1a}=2k_{1b}/3$. Control parameter values: $\tau=21$, $k_{1a}=0.2$, and $k_{1b}=0.3$.

nals and the interaction can be bidirectional (similar to the previous examples) or unidirectional.

An example for bidirectional coupling is shown in Fig. 7. To improve the readability the control cells used are marked white only for the transient phase shown in Fig. 7(a). For the final, asymptotic behavior only the rectangular envelope of the line segments is plotted to enable a look at the occuring identical synchronization within the region of control cells for $k_{1a}=0.19$, $k_{1b}=0.3$, and $\tau=134$.

To analyze the synchronization process at the control cells in more detail we shall compare now horizontal sections (x,y_l) and (x,y_u) of the spatial domain shown in Fig. 7 at the middle of the lower and the upper line segment of control cells, given by $y_l=\{-76,-75\}$ and $y_u=\{38,39\}$, respectively. The synchronization error

$$\mathbf{e}(x,t)=\mathbf{f}((x,y_l),t)-\mathbf{f}((x,y_u),t) \tag{22}$$

is an indicator of the quality of synchronization of regions close to both rows of control cells. Figure 8 shows examples for a successful synchronization of the GLE (3) using bidirectional [Figs. 8(a)–8(c)] or unidirectional [Figs. 8(d)–8(f)] coupling. As can be seen in Figs. 8(a) and 8(d) in both cases the synchronized state is reached after short transients once the control signal is activated at $t=30$. Figures 8(b) and 8(e) show the asymptotic synchronization error as a function of the horizontal distance d_x of control cells within the line segments that must not exceed the spatial correlation length $C_{xy}\approx 8.5$ for successful synchronization over the full width of line segments. Figures 8(c) and 8(f) show the dependence of the synchronization errors on the feedback gains k_{1a}, k_{1b} for $d_x=d_y=C_{xy}/2$, where k_{1a} and k_{1b} are increased simultaneously with a fixed relation $k_{1a}=2k_{1b}/3$.

Note that synchronization occurs here only locally in the vicinity of the control cells. This feature is visualized in Fig. 9. Figure 9(a) shows two line segments of control cells where the cells of the lower segment drive those of the upper segment (similar to Fig. 7). Figure 9(b) shows a second 2D GLE with the same spatial domain and boundary conditions like in Fig. 9(a) but different initial conditions. The white rectangular segment of control cells in Fig. 9(b) is driven by cells from the lower segment in Fig. 9(a) using the parameter $k_{1b}=0.3$ and the control signals $u_{1u}=k_{1b}s_{1l}(t)$ and $u_{2u}=k_{1b}s_{1l}(t)$ applied to the upper cells in Figs. 9(a) and 9(b), respectively. Figure 9(c) shows the difference of both GLEs where the synchronized region is clearly visible as a homogeneously shaded area.

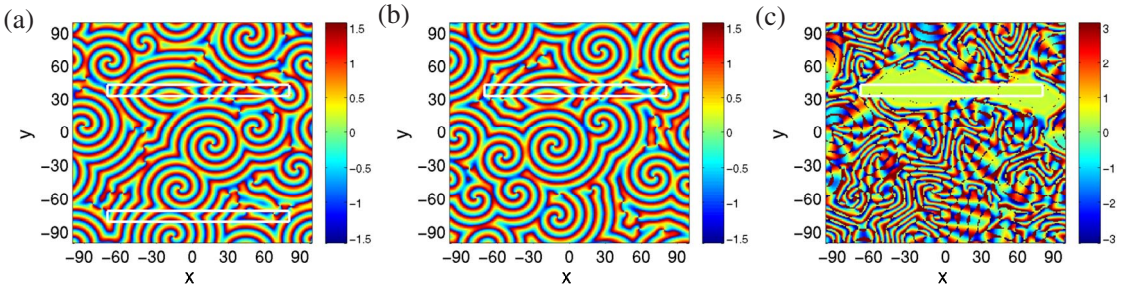

FIG. 9. (Color online) Phase dynamics of two coupled and synchronized GLEs (3). Control cells in the lower rectangular segment in (a) drive corresponding cells in the upper segments (compare Fig. 7) in (a) and (b). (c) Differences of state variables of (a) and (b) indicating a region of synchronization in the vicinity of the upper segments.

IV. CONCLUSION

Delayed feedback control using several different delay times provides many possibilities to control and manipulate spatiotemporal dynamics. We presented examples where the complex Ginzburg-Landau equation is controlled with spatially varying gain factors (inhomogeneous control) or control is applied only locally in space at some control cells. In the latter case the original system is perturbed only weakly but still new dynamics are generated with a different (target) pattern occurring. The dynamics of the control cells are synchronized due to the (local) coupling imposing new dynamical boundary conditions. This interplay between control, spatiotemporal structure formation, and synchronization is an interesting topic for future work on delayed feedback control of spatially extended systems.

[1] M. C. Cross and P. C. Hohenberg, Rev. Mod. Phys. **65**, 851 (1993).
[2] S. Jakubith, H. H. Rotermund, W. Engel, A. von Oertzen, and G. Ertl, Phys. Rev. Lett. **65**, 3013 (1990).
[3] M. Kim *et al.*, Science **292**, 1357 (2001).
[4] M. Bertram and A. S. Mikhailov, Phys. Rev. E **67**, 036207 (2003).
[5] T. Frisch, S. Rica, P. Coullet, and J. M. Gilli, Phys. Rev. Lett. **72**, 1471 (1994).
[6] F. H. Fenton, E. M. Cherry, H. M. Hastings, and S. J. Evans, Chaos **12**, 852 (2002).
[7] H. Varela, C. Beta, A. Bonnefont, and K. Krischer, Phys. Rev. Lett. **94**, 174104 (2005).
[8] G. Hu, J. Xiao, L. O. Chua, and L. Pivka, Phys. Rev. Lett. **80**, 1884 (1998).
[9] A. S. Mikhailov and K. Showalter, Phys. Rep. **425**, 79 (2006).
[10] I. V. Biktasheva, Phys. Rev. E **62**, 8800 (2000).
[11] I. Aranson, H. Levine, and L. Tsimring, Phys. Rev. Lett. **72**, 2561 (1994).
[12] R. M. Mantel and D. Barkley, Phys. Rev. E **54**, 4791 (1996).
[13] V. Petrov, Q. Ouyang, and H. L. Swinney, Nature (London) **388**, 655 (1997).
[14] S. Alonso, F. Sagues, and A. S. Mikhailov, Science **299**, 1722 (2003).
[15] A. V. Panfilov, S. C. Müller, V. S. Zykov, and J. P. Keener, Phys. Rev. E **61**, 4644 (2000).
[16] N. Garnier, R. O. Grigoriev, and M. F. Schatz, Phys. Rev. Lett. **91**, 054501 (2003).
[17] K. Pyragas, Phys. Lett. A **170**, 421 (1992).
[18] J. E. S. Socolar, D. W. Sukow, and D. J. Gauthier, Phys. Rev. E **50**, 3245 (1994).
[19] M. E. Bleich and J. E. S. Socolar, Phys. Rev. E **54**, R17 (1996).
[20] D. Battogtokh and A. Mikhailov, Physica D **90**, 84 (1996).
[21] M. Münkel, F. Kaiser, and O. Hess, Phys. Rev. E **56**, 3868 (1997).
[22] V. S. Zykov, A. S. Mikhailov, and S. C. Müller, Phys. Rev. Lett. **78**, 3398 (1997).
[23] J. Schlesner, V. Zykov, H. Engel, and E. Schöll, Phys. Rev. E **74**, 046215 (2006).
[24] N. Baba, A. Amann, E. Schöll, and W. Just, Phys. Rev. Lett. **89**, 074101 (2002).
[25] A. Ahlborn and U. Parlitz, Phys. Rev. Lett. **93**, 264101 (2004).
[26] Similar stabilizing features have recently been reported for chaotic coupled maps with random delays by C. Masoller and A. C. Marti, Phys. Rev. Lett. **94**, 134102 (2005).
[27] A. Ahlborn and U. Parlitz, Phys. Rev. E **72**, 016206 (2005).
[28] A. Ahlborn and U. Parlitz, Opt. Lett. **31**, 465 (2006).
[29] A. Ahlborn and U. Parlitz, Phys. Rev. E **75**, 065202(R) (2007).
[30] I. Harrington and J. E. S. Socolar, Phys. Rev. E **64**, 056206 (2001).
[31] L. Junge and U. Parlitz, Phys. Rev. E **61**, 3736 (2000).
[32] The phase of the complex solution $f(\mathbf{x},t)$ is restricted here to the interval $[0,\pi]$.